UDC 666.1.031.13:532.5

EFFECT OF AN OVERFLOW SILL ON HEAT AND MASS TRANSFER IN THE GLASS-MELTING TANK OF A FURNACE WITH HORSESHOE-SHAPED FLAME

V. Ya. Dzyuzer[1] and V. S. Shvydkii[1]

Translated from Steklo i Keramika, No. 7, pp. 6 – 12, July, 2006.

A numerical model is used to study the effect of the height and position of an overflow sill on glass melt hydrodynamics and heat transfer in a glass-melting tank furnace. A differentiated effect of the overflow sill on the formation of convection flows and heat and mass transfer in various parts of the tank is established. It is demonstrated that the considered parameters of the sill have virtually no effect on the intensity of the charge convection cycle. At the same time, they have a significant effect on melt hydrodynamics past the sill. The quantitative correlations between the design parameters of the sill and certain characteristics of heat and mass transfer in the melting tank are identified.

An overflow sill in the melting tank is an obligatory element of contemporary glass-melting furnaces. Physical modeling of melting tank hydrodynamics has provided a qualitative understanding of its role in convection flows [1, 2]. At the same time, it should be noted that the limitations of this method do not provide reliable quantitative information needed for design work. The quantitative regularities of the effect of this structural element on the melt flow pattern and temperature field can be obtained using contemporary computer simulation technologies, for instance a numerical model of melting tank hydrodynamics [3, 4]. Computations have been performed for the following linear sizes of the melting tank (m): $L_{mt} = 13.62$, $h_1 = 1.3$, $h_n = 0.3$, and $b_s = 0.4$ (Fig. 1) The overflow sill height h_s was taken equal to 0.2, 0.4, 0.6, 0.8, 1.0, and 1.1. m. The longitudinal coordinate of the sill remained constant for all variants: $x_s = 9.2$ m. The location of the sill along the melting tank varied within the limits of $x_s / L_{mt} = 0.44 – 0.91$ ($x_s = 6.0 – 12.4$ m) with a step of 0.4 m; the sill height remained constant, $h_s = 0.8$ m. Other initial data and boundary conditions for modeling are specified in [4 – 6].

The results of numerical modeling are represented by two-dimensional fields of relative streamlines and glass melt temperatures. Streamlines are normalized with respect to the mass flow rate of glass through the tank neck equal to 3.47 kg/sec. For a clear representation of flow patterns in different parts of the tank, the scale variation method was applied. The furnace output of 300 tons/day accepted in the computations is achieved by a specific glass melt output equal to 2.6 tons/m^2 per day. The glass melt temperature distribution t_{gm} on the tank surface is specified by the regression equation obtained on the condition that the total flame length $l_f – L_{mt}$ (the length of the visible part of the flame is $0.7L_{mt}$, i.e., $x = 9.534$ m) [7]:

$$t_{gm}(x, y) = 1145.23 + 87.11x + 32.76y – 19.51x^2 – 1.24xy – 12.96y^2 + 0.13x^2y + 0.18xy^2 – 0.02x^2y^2 + 2.55x^3 + 1.95y^3 – 0.11x^4 – 0.10y^4,$$

where x and y are the longitudinal and lateral coordinates of the tank, m.

In two-dimensional setting the temperature distribution on the glass melt surface is specified by the expression obtained by averaging the following equation across the tank width:

$$\bar{t}_{gm_{\Delta x}} = 1236.2847 – 1.805463x + 6.689836x^2 – 0.22151479x^3 – 0.01641339.$$

It has been established earlier [5, 8] that the regularities of the melt flow in the tank without a dividing sill and in the

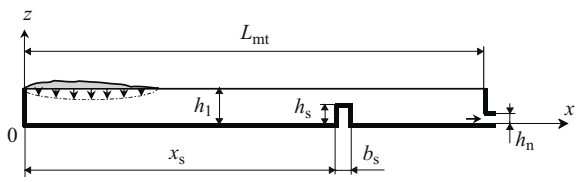

Fig. 1. Calculation scheme of the longitudinal section of the melting tank of a glass-melting furnace with horseshoe-shaped flame.

[1] Ural State Technical University (UPI), Ekaterinburg, Russia.

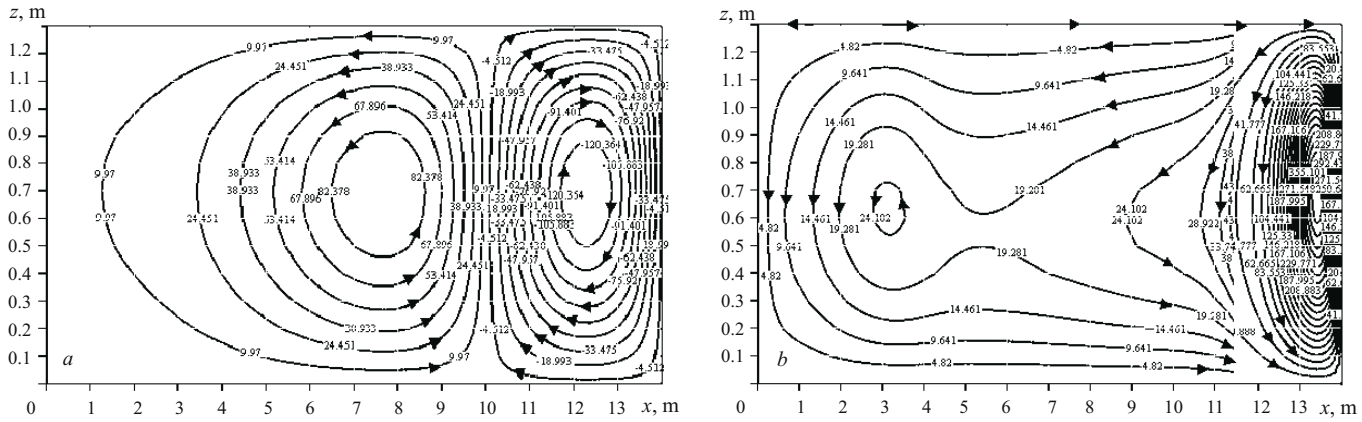

Fig. 2. Glass melt pattern in the longitudinal section of the tank: *a*) under natural convection; *b*) in the presence of a working flow and $h_s = 0$.

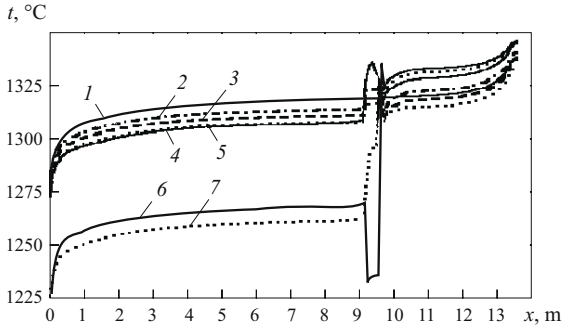

Fig. 3. Variation of glass melt temperature in the bottom layer of the tank: *1*, *2*, *3*, *4*, *5*, *6*, and *7*) h_s = 0, 0.6, 0.4, 0.2, 0.8, 1.1, and 1.0 m, respectively.

absence of a working glass melt flow fully correspond to the classical concept of free thermogravitational convection in a medium heated from above [9]. In this case the temperature maximum on the heated surface is fully manifested as the contour-forming factor with the classical sense of rotation of the glass melt in the contours (Fig. 2*a*).

In a real glass-melting furnace where the melt flow is directed toward the tank neck, the temperature field on its surface is not the deciding mass transfer factor in the melting tank. A set of factors influence the formation of circulation contours in their sense of rotation [8]. The most significant factors are the conditions of the primary melt arriving at the tank (downwards near the left wall) and the withdrawal of the glass melt from the tank bottom near the right wall. The combination of these two factors is responsible for the formation of a single circulation contour with counterclockwise rotation (Fig. 2*b*). As the amount of the glass melt in the tank exceeds many times its flow rate via the neck per second, its greater part is forced to return to the circulation contour moving upwards along the right wall. A certain part of this "returned" glass melt gets into the main contour and migrates to the charging hopper. However, the greater part of the melt, due its continuous withdrawal, high temperature, and low viscosity, remains near the flow-through wall of the tank. It forms a local circulation subcontour with the same sense of rotation as the main contour. Note that the surface melt flow directed toward the neck to a certain extent conceals the details of the above pattern from observation.

Clearly the existence of a temperature maximum on the glass melt surface contributes to the formation of circulation in the left contour. However, the right contour is formed exclusively due to the bottom withdrawal of the melt for working. It should be stressed that the circulation intensity near the neck is higher by an order of magnitude that the intensity in the left part of the tank. Therefore, the glass melt temperature in the bottom layer near the neck reaches rather high values (Fig. 3). Due to the intense circulation, the temperature field in this part of the tank is relatively homogeneous. The mean integral temperature of the glass melt in the neck is $\bar{t}_{gm_n} = 1347°C$ and the bottom layer temperature varies within the limits of 1298 – 1338°C.

The installation of an overflow sill clearly modifies the flow pattern, since additional kinetic energy losses occur at this sill. Stalling is observed on the sharp edges of the sill top, which is typical of poorly streamlined bodies. On a sill with certain parameters local circulation contours with clockwise rotation may be formed. At the same time, the main regularities of the glass melt flow described above are preserved.

Figure 4*a* shows the glass melt flow pattern for the sill of height 0.2 m. It can be seen that this height is too small for the formation of an additional circulation contour, since the sill is totally inside the boundary layer. However this height is sufficient for modifying some fragments of the flow regularities. The additional obstacle to the flow separates a part of the glass melt volume and forms a closed local inner contour. Starting with $h_s = 0.4$ m we observe complete separation of the left and right circulation contours. With the sill of this height, a local circulation contour is formed near the left wall of the sill (Fig. 4*b*).

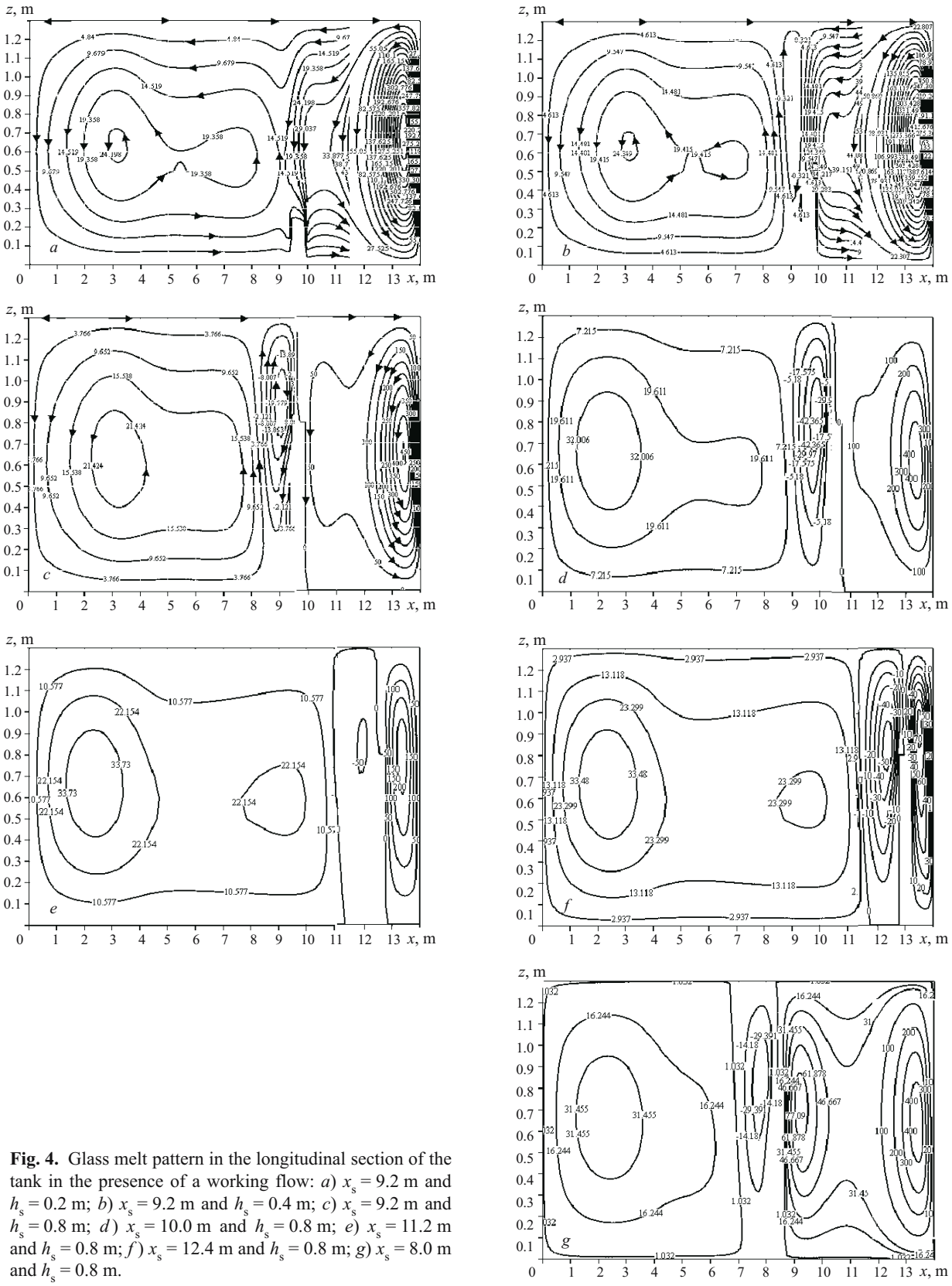

Fig. 4. Glass melt pattern in the longitudinal section of the tank in the presence of a working flow: *a*) x_s = 9.2 m and h_s = 0.2 m; *b*) x_s = 9.2 m and h_s = 0.4 m; *c*) x_s = 9.2 m and h_s = 0.8 m; *d*) x_s = 10.0 m and h_s = 0.8 m; *e*) x_s = 11.2 m and h_s = 0.8 m; *f*) x_s = 12.4 m and h_s = 0.8 m; *g*) x_s = 8.0 m and h_s = 0.8 m.

The above regularities are manifested most clearly when the sill height is above 0.4 m. In this case the total convection field is subdivided into three main circulation contours (Fig. 4*c*). A large asymmetric contour with the counterclockwise rotation is formed in the left part of the tank ($x \approx 0 – 8.2$ m). The contour pole is located at the point with

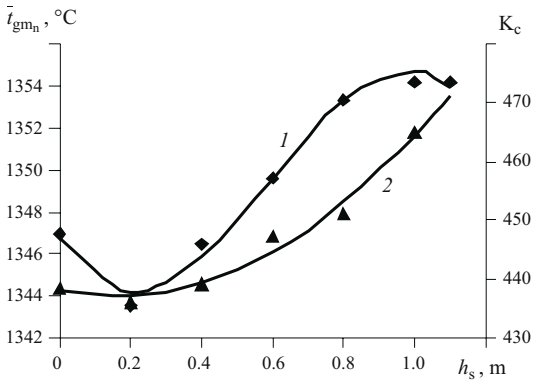

Fig. 5. The effect of the height of the overflow sill on the mean integral temperature of the flow in the neck $\bar{t}_{gm_n}$ (*1*) and its circulation multiplicity past the sill K_c (*2*).

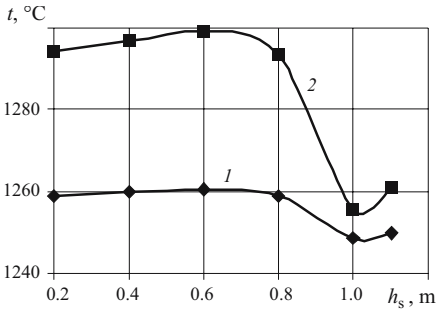

Fig. 6. The effect of the sill height on the glass melt temperature near the tank surface: *1*) $x = 2$ m, $z = 1.2$ m; *2*) $x = 2$ m, $z = 1.1$ m.

the coordinate $x \approx 3$ m and $z \approx 0.65$ m. The circulation multiplicity in this contour is not high and amounts to $k_1 = 40.63$. The second (smaller) contour with the clockwise glass melt rotation is adjacent to the left side of the overflow sill. In the upper part of the tank it reaches the middle of the sill ($x = 9.4$ m). The circulation multiplicity in this contour is slightly higher and amounts to $k_2 = 50.84$. Finally, to the right of the sill (in the upper part of the tank in starts from the middle of the sill) is the third circulation contour k_3 with counterclockwise rotation.

The glass melt circulation beyond the sill is induced by at least three simultaneous factors: the sill, the temperature gradient on the tank surface directed oppositely from the maximum, and the glass melt withdrawal via the neck. This is responsible for the formation of two subcontours in the third circulation contour, which have different coordinates of the poles and different circulation multiplicity. For the first circulation pole $x \approx 10.2$ m, $z \approx 0.7$ m, and $k_{3.1} = 98.63$; for the second pole $x \approx 13$ m, $z \approx 0.6$ m, and $k_{3.2} = 453.1$.

Note that the flow pattern shown in Fig. 4*c* is preserved for any height of the sill. Flow variations related to an increasing sill height are manifested in the quantitative parameters of the convection flows. An increase in h_s intensifies the local additional contour k_2 and the glass melt circulation near the neck $k_{3.2}$. In Fig. 5 the circulation multiplicity near the flow-through wall is denoted as K_c. If the third contour is not split into subcontours, then K_c is equivalent to k_3. In the case of two subcontours, K_c is equivalent to $k_{3.2}$.

Up to a certain height of the sill the temperature state in the left part of the tank (in front of the sill) weakly changes as h_s increases. This is clearly seen from the data in Fig. 3 illustrating the glass melt temperature variation in the bottom layer. The exception of the sills of height 1.0 and 1.1 m from this regularity is due to purely hydrodynamic reasons. At $h_s = 1.0$ m the distance from the sill top to the glass melt surface is equal to the neck height: $h_1 - h_n = h_2$. In this case the high-temperature melt stops flowing from the right part of the tank into the left part. As a consequence, the mean glass melt temperature in front of the sill decreases, whereas the circulation multiplicity past the sill grows. Note that the sill height equal to 1 m is the maximum admissible height ensuring a uniform temperature field in front of the tank neck. At $h_s = 1.1$ m the resistance of the sill is so high that the circulation multiplicity past the sill perceptibly decreases (by about 6%).

Summarizing the above, it can be stated that the installation of an overflow sill causes two changes in heat transfer. First, some heat is lost on the sill and, consequently, the mean glass melt temperature in the working zone is expected to decrease. Second, at $h_s > 0.4$ m, the proximity of its top to the melt surface is manifested, which raises the glass melt temperature in the neck. Due to the combined effect of these regularities, the temperature level initially decreases with increasing h_s and grows (Fig. 5). The observed regularities can be described by the expression:

$$\bar{t}_{gm_n} = 1346.753 - 26.97h_n + 80.179h_n^2 - 45.253h_n^3.$$

Note the close correlation of the circulation multiplicity and the barrier height and with the glass melt temperature in the neck:

$$K_c = 438.04 - 11.4335h_n + 37.7768h_n^2;$$

$$\bar{t}_{gm_n} = 13.483K_c - 0.014575K_c^2 - 1763.86.$$

Let us consider the effect of the sill height on heat transfer in the left part of the tank (before the barrier). The data in Fig. 3. indicate that the installation of a sill decreases the temperature of the bottom glass melt layers. The most perceptible decrease in temperature is observed in the case of a high sill ($h_s = 1.0$ and 1.1 m). The observed regularity is caused by the effect of the sill height on melt hydrodynamics. The tendency to the separation of the left and right circulation contours upon installing the sill decreases the quantity of high-temperature melt returned from the right part of the tank to the melting zone. With a high sill ($h_s = 1.0$, and 1.1 m) the replenishment of the left contour stops com-

pletely, which is expressed in the low level of the bottom temperature.

The above to a certain time is corroborated by the data in Fig. 3 showing the variation of the glass melt temperature in the center of the site of primary melt formation (x = 2.0 m). We consider the temperature of two points located at 100 and 200 mm from the tank surface (z = 1.2 and 1.1 m, respectively). These points are chosen due to the dominant role of the lower heat front in melting batch portions charged into the furnace. Note that the variation of the sill height in the limits of h_s = 0.2 – 0.6 m does not perceptibly modify the melting temperature. An increase in the sill height to 1.1 m is accompanied by a perceptible decrease in the glass temperature from 1260.4 to 1249.9°C (z = 1.2 m) and from 1299.1 to 1261.0°C (z = 1.1 m).

Analysis of the hydrodynamics and heat transfer suggests some definite conclusions on the ultimate height of the sill for the accepted boundary conditions in modeling. In the context of hydrodynamics, the sill height should satisfy the expression:

$$(h_1 - h_2) > h_s > h_2 .$$

Taking into account heat transfer in the melting part of the tank this expression can be refined by the relationship

$$(h_1 - 2h_n) \geq h_s \geq 2h_n .$$

Considering the effect of the sill location on melt hydrodynamics, let us take the reference variant ($l_f = L_{mt}$, x_s = 9.2 m, and h_s = 0.8 m) whose flow pattern is shown in Fig. 4*c*. Note that the longitudinal coordinate (x = 10.0 m) of the maximum temperature of the glass melt surface (1501.6°C) in this variant [5] does not coincide with the coordinate of the left (and the right) wall of the overflow sill (x_s = 9.2 and 9.6 m).

When the longitudinal coordinate of the sill (x_s = 10 m) coincides with the temperature maximum on the melt surface, the flow pattern remains qualitatively unchanged. At the same time, two regularities can be identified (Fig. 4*d*). Firstly, the first circulation contour in front of the sill exhibits a tendency to the formation of the second circulation pole, i.e., splitting into two subcontours $k_{1.1}$ and $k_{1.2}$. Secondly, the size of the left subcontour of the third contour (beyond the sill) decreases until it actually vanishes: $k_{3.1} \to 0$.

The circulation multiplicity in the main pole of the left contour remains unchanged and equal to $k_{1.1}$ = 40.63. The second pole is formed at the point with coordinates $x \approx 5.6$ m and $z \approx 0.6$ m. The circulation multiplicity in this pole is k1.2 = 21.035. In the second contour, k_2 grows to 54.76. As for the third contour, due to the disappearance of the left subcontour and the general decrease in the glass melt volume past the sill, the circulation multiplicity increases to k_3 = 453.44.

A further shift of the sill to the right (x_s > 10 m) predictably changes the glass flow pattern. The circulation multiplicity in the second pole of the first contour and in the second contour will increase. Circulation multiplicity in the third contour will initially increase. However, starting with a certain coordinate of the sill position, the circulating flow is delayed by friction and the circulation multiplicity decreases. The second reason for decreasing the circulation multiplicity in the third contour is the decrease of the glass melt volume beyond the sill.

The above statement is illustrated by the data in Fig. 4*e* showing the melt flow pattern where the coordinate of the left plane of the sill is 11.2 m. Here the circulation multiplicity at the second pole of the first contour increases to $k_{1.2}$ = 22.625, in the second contour — to k_2 = 58.88, and in the third contour starts decreasing and is equal to k_3 = 466.17 (its maximum value is equal to 469.46).

With the maximum shift of the barrier (x_s = 12.4 m) the circulation muliplicities are (Fig. 4*f*): at the left pole of the first contour $k_{1.1}$ = 40.69, at the right pole of the first contour $k_{1.2}$ = 24.49, in the second contour k_2 = 58.15, and in the third contour (past the sill) k_3 = 74.21.

In glass-melting practice the most interesting parameters are the glass temperature in the tank neck and its distribution along the neck height (z = 0, 0.1, 0.2, and 0.3 m). The physical interpretation of the revealed regularities is clear. Since the glass melt temperature in the right part of the tank decreases (with x > 10.0 m), the mean temperature on the site ranging from the left plane of the sill to the flow-through wall of the tank decreases as well. The mean glass melt surface temperature $\bar{t}_{gm_{\Delta x}}$ on the segment $\Delta x = L_{mt} - (x_s + b_s)$ exibits a certain dependence on the site of the sill installation:

$$\bar{t}_{gm_{\Delta x}} = 1682.3379 - 96.082927 x_s + 13.718138 h_s^2 - 0.64982804 h_s^3 .$$

Since the melt penetrates into the neck mainly from the right part of the tank (after the barrier), the nearer the barrier is to the flow-through wall, the lower is the mean glass melt temperature in the neck. The relation between the specified mean temperatures is nonlinear due to the effect of circulation multiplicity, whose increase facilitates the homogenization of temperatures. With correlation coefficient r = 0.999950 and standard deviation s = 0.128°C it is described by the fifth power polynomial:

$$\bar{t}_{gm_n} = -136079.3 + 2736.3534 \bar{t}_{gm_{\Delta x}} - 0.95165341 \bar{t}^{\,2}_{gm_{\Delta x}} - 0.0013737715 \bar{t}^{\,3}_{gm_{\Delta x}} + 1.203336 \times 10^{-6} \bar{t}^{\,4}_{gm_{\Delta x}} - 2.7080236 \times 10^{-10} \bar{t}^{\,5}_{gm_{\Delta x}} .$$

In principle, with a slightly lower correlation coefficient (r = 0.999258) and a slightly higher mean quadratic deviation (s = 0.383°C) it is possible to use a cubic polynomial:

$$\bar{t}_{gm_n} = -96005.46 + 204.86861 \bar{t}_{gm_{\Delta x}} - 0.14382646 \bar{t}^{\,2}_{gm_{\Delta x}} - 3.3684764 \times 10^{-5} \bar{t}^{\,3}_{gm_{\Delta x}} .$$

TABLE 1

x_s, m	t_{gm_n}, °C, at z, m				$\bar{t}_{gm_n}$, °C	σ,* °C	K_c
	0	0.1	0.2	0.3			
9.2	1344.8	1352.7	1353.0	1353.2	1351.57	4.088500	453.10
9.6	1344.3	1352.2	1352.5	1352.6	1351.06	4.070217	451.38
10.0	1343.3	1351.2	1351.5	1351.6	1350.02	4.070217	453.44
10.4	1341.7	1349.6	1349.9	1350.1	1348.45	4.088500	461.56
10.8	1339.5	1347.4	1347.7	1347.9	1346.28	4.088500	469.46
11.2	1337.5	1345.4	1345.6	1345.8	1344.20	4.053291	466.17
11.6	1334.7	1342.6	1342.8	1342.8	1341.36	4.017773	401.62
12.0	1330.8	1338.6	1338.6	1338.0	1337.17	3.810512	230.53
12.4	1321.5	1329.3	1328.8	1327.3	1327.52	3.585503	74.21

* σ is the mean quadratic deviation of local (nodal) temperature t_{gm_n} from its mean integral value in the tank neck $\bar{t}_{gm_n}$.

TABLE 2

x_s, m	First contour,* $k_{1.2}$	Second contour, k_2	Third contour		$\bar{t}_{gm_{\Delta x}}$, °C
			$k_{3.1}$	$k_{3.2}$	
6.0	–	34.41	64.51	448.15	1448.59
7.0	–	39.60	73.64	454.22	1455.05
8.0	–	44.60	84.60	457.38	1457.95
8.4	–	46.66	89.29	457.01	1457.59
8.8	–	48.75	93.88	455.46	1456.15
9.2	–	50.84	98.63	453.10	1453.45
9.6	20.67	52.86	104.55	451.38	1449.30
10.0	21.04	54.76	–	453.44	1443.51
10.4	21.49	56.52	–	461.56	1435.85
10.8	22.03	57.94	–	469.46	1426.11
11.2	22.62	58.88	–	466.17	1414.04
11.6	23.25	59.20	–	401.62	1399.39
12.0	23.88	58.88	–	230.53	1381.87
12.4	24.49	58.15	–	74.21	1361.22

* For all variants $k_{1.1}$ = 40.63 – 40.69.

If the thermal homogeneity of the melt in the neck is characterized by temperature dispersion or standard deviation, we see an obvious correlation of the mean glass melt temperature and its standard deviation with the position of the overflow sill. Table 1 gives initial data reflecting these correlations.

Obviously, the reverse situation, i.e., moving the barrier toward the charging hopper, is of interest as well. Based on the above data, two major changes can be expected. First, the second pole of the first contour will completely disappear and the first (left) pole of the third contour, on the contrary, will be manifested more clearly. Second, the circulation multiplicity in the second contour will decrease.

Figure 4*g* shows the flow pattern at x_s = 8.0 m, i.e., where the left wall of the sill is located 2.0 m to the left from the maximum surface temperature. We can observe the complete confirmation of the assumptions made.

Generally, the qualitative changes of the glass melt behavior with different positions of the overflow sill have a physical explanation. It is more difficult to interpret the variations of the quantitative parameters. Table 2 shows the integral parameters of melt hydrodynamics for different locations of the sill. The last column lists the mean glass melt temperatures on the site ranging from the left plane of the sill to the right wall of the tank. The reasons for precisely such variation of glass melt hydrodynamic parameters requires additional investigation.

To conclude, it should be noted that the height and location of the overflow sill have a differentiated effect on heat and mass transfer in various parts of the melting tank. It can be stated that the considered parameters of the sill have a weak effect on the intensity of the charge convection cycle of the melt. Therefore, installing a sill cannot be regarded as an effective instrument for batch melting and producing primary melt. At the same time, this design element has a powerful effect on the melt hydrodynamics past the sill. It increases the melt circulation multiplicity after the sill and raises the melt temperature in the neck. In other words, the presence of an overflow sill of a certain height increases the homogeneity of the melt and extends its stay in the tank, which has a positive effect on the quality of the finished glass melt. In the first approximation, when selecting the height of the sill one can be guided by the relationship

$$(h_1 - 2h_n) \geq h_s \geq 2h_n .$$

The optimum h_s value is determined taking into account the specific output of the furnace and the glass melt temperature restrictions in the working zone.

It is more complicated to select a site for the sill installation. If we consider it as an instrument of quellpunkt formation, the position of the sill in the tank should coincide with the temperature maximum on the melt surface. Taking this approach, the determination of the longitudinal coordinate of the sill involves solving a multifactor problem whose variables include the furnace efficiency and thermal power, the chemical composition of glass, the melting tank geometry, the heat losses via the brickwork, and other parameters. One should also determine the role of the additional circulation contour formed on the left plane of the barrier.

Generally, the considered results demonstrate, on the one hand, the advisability of having an overflow sill in the melting tank and, on the other hand, the need to justify its height and location.

REFERENCES

1. V. A. Tolstov, V. N. Kiselev, S. S. Denisova, et al., "Physical modeling of glass melt hydrodynamics in a high-efficiency furnace for melting container glass," *Steklo Keram.*, No. 8, 14 – 17 (2000).
2. A. S. Kozlov, S. B. Lisenenkova, N. A. Gusev, et al., "Glass melt hydrodynamics in a regeneration furnace," *Steklo Keram.*, No. 2, 6 – 8 (1984).

3. V. Ya. Dzyuzer and V. S. Shvydkii, "Numerical modeling of melt flow in glass-melting furnaces," in: *Control Mechanisms and Processes, Vol. 1. Proc. 34th Ural Seminar* [in Russian], Izd-vo UrO RAN, Ekaterinburg (2004), pp. 125 – 136.
4. V. Ya. Dzyuzer and V. S. Shvydkii, "Mathematical model of hydrodynamics of the melting tank in a glass-melting furnace," *Steklo Keram.*, No. 1, 3 – 8 (2005).
5. V. Ya. Dzyuzer and V. S. Shvydkii, "The effect of flame length on melting tank hydrodynamics in a glass-melting furnace with horseshoe-shaped flame," *Steklo Keram.*, No. 9, 5 – 11 (2005).
6. V. Ya. Dzyuzer and V. S. Shvydkii, "Establishing boundary conditions for the problem of melt hydrodynamics in a glass-melting furnace," in: *Proc. 25th Russian School and 35th Ural Seminar, Part 1. Science and Technology* [in Russian], Izd-vo RAN, Moscow (2005), pp. 174 – 180.
7. V. Ya. Dzyuzer and V. S. Shvydkii, "The effect of flame length on external heat transfer in a glass-melting furnace with horseshoe-shaped flame," *Steklo Keram.*, No. 7, 3 – 7 (2005), pp. 181 – 190.
8. V. Ya. Dzyuzer and V. S. Shvydkii, "A study of heat and mass transfer in a melting tank of a glass-melting furnace," in: *Proc. 25th Russian School and 35th Ural Seminar, Part 1. Science and Technology* [in Russian], Izd-vo RAN, Moscow (2005).
9. A. V. Lykov and B. M. Berkovskii, *Combustion and Heat Waves* [in Russian], Énergiya, Moscow (1974).